165 HIGH-RESOLUTION PHASED ARRAY RADAR OBSERVATIONS OF AN OKLAHOMA HAILSTORM PRODUCING EXTREMELY-LARGE HAIL

ARTHUR WITT*

NOAA/National Severe Storms Laboratory, Norman, OK

1. INTRODUCTION

On 31 May 2013, an outbreak of severe thunderstorms occurred across central OK, resulting in some of the most extreme tornado and hail events recorded to date. These included an EF3 tornado with a maximum damage width of 4.2 km (2.6 mi), along with hailstones up to 160 mm in diameter (Fig. 1). Prior to 31 May 2013, the five largest verifiable hailstones in the United States ranged from 203 mm to 152 mm in diameter (Blair and Leighton 2012). This would rank the 160 mm hailstone observed on 31 May 2013 as the (new) fifth largest in the U.S. (the fourth largest being 175 mm in diameter). The 160 mm hailstone fell on the west side of El Reno, OK, placing it within 60 km of the National Weather Radar Testbed Phased Array Radar [NWRT PAR (Zrnic et al. 2007); hereafter PAR] located in Norman, OK. The close proximity to the PAR allowed for high-resolution (in both space and time) Doppler radar observation of the supercell storm that produced the 160 mm hailstone, from the time of storm initiation (first echo $\geq$ 15 dBZ) at 2119 UTC through the storm's movement across El Reno (2300–2310 UTC).

2. METHODS

a. 160 mm hailstone

The 160 mm hailstone was reported via social media (Hyvärinen and Saltikoff 2010) on the KFOR-TV web page (photo #25 in the gallery at http://kfor.com/2013/06/04/update-el-reno-union-city-tornado-widest-tornado-on-record/). It fell at the home of C. Parker (926 S. Magnolia Street; latitude 35.5227°, longitude −97.9755°), located 304° and 56 km from the PAR. Although the source and location of the hail report are known, no time was mentioned as to when the hailstone actually fell. However, it was possible to obtain a reasonably accurate estimate of ~2305 UTC as the time that the hailstone fell, based on both WSR-88D dual-polarization and PAR radar signatures as the storm crossed the location of the report. The dual-polarization signatures (Kumjian and Ryzhkov 2008), from the KCRI WSR-88D in Norman, included a deep vertical column of low copolar cross-correlation coefficient (ρ_{HV}; Fig. 2), along with a relative minimum in low-altitude differential reflectivity (Z_{DR}; Fig. 3).

FIG. 1. Photo of the 160 mm hailstone.

b. Radar-based parameters

Storm characteristics were assessed via a variety of radar parameters. The velocity parameters were derived from the "base" velocity data (in its original spherical-coordinate form), with the reflectivity parameters determined after "mapping" the base reflectivity

Corresponding author address: Arthur Witt, NOAA/National Severe Storms Laboratory, 120 David L. Boren Blvd., Norman, OK, 73072.
E-mail: Arthur.Witt@noaa.gov

data to a 3D latitude-longitude-height grid at a resolution of 0.01° x 0.01° x 1.0 km (Lakshmanan et al. 2006). The reflectivity parameters examined included maximum reflectivity at the $-20°$C height (Z_{253K})[1], vertically integrated liquid water content (VIL; Amburn and Wolf 1997), and maximum expected size of hail (MESH; Witt et al. 1998; Lakshmanan et al. 2007). The velocity parameters examined included the maximum storm-top divergent outflow (STD; Witt and Nelson 1991) and maximum mid-altitude rotational velocity (MRV; Witt 1998). The STD and MRV were calculated as:

$$STD = V_{max} - V_{min} \quad (1)$$

$$MRV = (V_{max} - V_{min})/2 \quad (2)$$

where V_{min} and V_{max} are the peak inbound and outbound velocities in the storm's divergence and rotation signatures. To minimize errors in the measurement of STD and MRV, only base velocity data with corresponding reflectivity $\geq$ 15 dBZ and spectrum width $<$ 13 m s^{-1} were used. An additional criterion, to avoid use of unreliable data, was that a candidate velocity have sufficient spatial continuity with neighboring velocities on the same elevation scan, defined here as at least one adjacent velocity value within 5 m s^{-1} of the candidate velocity value. In the calculation of STD, V_{min} could come from either the same or the next higher elevation scan as V_{max}, with V_{min} at the next higher elevation scan most often being used for STD signatures at closer distances to the radar (to reduce the altitude difference between V_{min} and V_{max}).

3. STORM ENVIRONMENT

The atmospheric environment across central OK on 31 May 2013 was typical of severe thunderstorm outbreaks, with the 1800 UTC OUN rawinsonde indicating very high Convective Available Potential Energy (CAPE) and strong vertical wind shear (Fig. 4). At 2100 UTC, a quasi-stationary front was located from southwestern OK to north-central OK, with surface air temperatures from 27–39°C (Fig. 5). Low-altitude moisture was highest across central OK just southeast of the front, with surface dewpoint temperatures up to 24°C (Fig. 5) and 850 mb dewpoint temperatures $>$18°C (Fig. 6). Also noteworthy at 850 mb was the strong temperature gradient across western OK, resulting in a region of enhanced warm air advection along the surface frontal zone. At mid-altitudes, a shortwave trough was located just west of OK, producing westerly winds $\sim$50 m s^{-1} across the northern half of the state (Figs. 4, 7). The El Reno storm initiated $\sim$120 km west of Norman in an area of maximum surface θ_e and moisture convergence (Fig. 5). As the storm moved east-northeast toward El Reno, it encountered increasing low-altitude inflow, with surface winds backing and strengthening (Fig. 8). By the time of the 0000 UTC OUN rawinsonde (Fig. 9), vertical wind shear had markedly increased, with storm-relative helicity values 2–3 times higher than those measured at 1800 UTC.

4. RADAR OBSERVATIONS

The first PAR detection of the El Reno storm occurred at 2119 UTC (274° and 118 km from the PAR; Fig. 10). Given an environment supportive of explosive growth, the storm rapidly intensified, with Z_{253K} increasing from 15 dBZ to 48 dBZ within 14 min (Fig. 11). A brief pause ensued, after which Z_{253K} further increased to 69 dBZ [35 min after first echo (AFE)]. In terms of VIL and MESH, they both increased rapidly from $\sim$11 min AFE to $\sim$35 min AFE. Following this initial period of rapid growth in both storm size and intensity, the storm continued to increase in size and volume, due to both expansion of the main storm cell and through merging with several other cells. However, storm intensity exhibited a more cyclical pattern, with relatively minor fluctuations in Z_{253K} (between 62 dBZ and 69 dBZ) and VIL (between 53 kg m^{-2} and 75 kg m^{-2}), and greater variations in MESH (first peaking at 82 mm, then dropping to 43 mm, up again to 78 mm, then down to 52 mm). At $\sim$70 min AFE (2230 UTC), the El Reno storm merged with another strong storm cell from the southwest (Fig. 12), after which it transitioned into an intense "classic" supercell (Rasmussen and Straka 1998), displaying a distinct hook echo, deep bounded weak echo region, and strong mesocyclone and tornadic vortex signatures (Fig. 13). There was also a large and rapid increase in MESH, from 52 mm at 79 min AFE to 121 mm at 86 min AFE (Fig. 11). The MESH then dropped to 85 mm, followed by another rapid increase to 118 mm at 100 min AFE. Following this secondary maximum in MESH, a large and rapid decrease occurred, with MESH falling to 53 mm at 110 min AFE.

The character of this pronounced "pulse" in MESH from 79 min AFE to 110 min AFE was examined in greater detail via a time-height plot of the reflectivity values used in its calculation (Fig. 14). The large increase in MESH from 79 min AFE to 86 min AFE was primarily due to increasing reflectivities at 7–10 km AGL, with reflectivities above 13 km AGL actually decreasing. Also noteworthy during this period was the near steady reflectivities at 1–2 km AGL, resulting in a pronounced increase in the vertical reflectivity

[1] The $-20°$C height was selected based on this being an important temperature for the growth of large hail (Nelson 1983).

gradient. This change in the vertical reflectivity profile is indicative of a strengthening updraft and building hail core aloft. Following this peak in reflectivity up to 74 dBZ at 7 km AGL, the vertical reflectivity gradient then steadily decreased as the elevated hail core descended, such that by the time of the relative minimum in MESH at 96 min AFE, there was little remaining difference in reflectivities below 13 km AGL. The final relative maximum in MESH (118 mm) at 100 AFE differed in character from the previous peak in that it was due primarily to increasing reflectivities in the upper altitudes of the storm, with reflectivity of 70 dBZ up to 12 km AGL and 59 dBZ up to 16 km AGL. It's likely that the 160 mm hailstone ultimately fell out of the storm from this high-altitude region, as this would allow for the growth needed to attain its final extremely-large size, given the long distance to the surface.

In terms of the velocity parameters, the STD followed a pattern similar to the reflectivity parameters, increasing rapidly during the explosive growth phase, followed by a more cyclic pattern during the middle, cell-merging, phase (Fig. 15). As the storm began to transition into a classic supercell $\sim$75 min AFE, a notable pulse in STD occurred, just prior to the rapid increase in MESH at $\sim$80 min AFE. This was then followed by a fairly steady increase in STD to a peak of 150 m s^{-1} at 110 min AFE. In contrast to the other radar parameters, the MRV increased at a more gradual, relatively steady pace, reaching a peak of 42.5 m s^{-1} at 107 min AFE.

5. DISCUSSION

The damage potential and threat to life and property associated with a severe storm increases at a nonlinear rate as the intensity of the storm increases. Hence, timely identification and warning on the occurrence of extreme severe-weather events is vital. The PAR's ability to rapidly scan a storm's full 3D volume allows for additional warning lead-time of such events. The occurrence of the 160 mm hailstone within 60 km of the PAR provides the opportunity to examine the character and evolution of the storm that produced such as huge hailstone in greater detail than would be possible from operational radars scanning at slower rates (e.g., the WSR-88D).

Given the environmental setting on 31 May 2013, it's not surprising that the El Reno storm rapidly intensified after first echo. Following this initial explosive growth phase, it went through a more "cyclic" phase during which it merged with several adjacent cells. Then, $\sim$30 min before occurrence of the 160 mm hailstone, it transitioned into a classic supercell.

During the 20–30 min period when growth and fallout from the storm of the 160 mm hailstone likely occurred, the El Reno storm exhibited exceptional structural features and radar-measured intensities (for the parameters examined here). The maximum STD of 150 m s^{-1} is the second largest documented STD observation, eclipsed only by the 157 m s^{-1} value seen in the Fort Cobb, OK storm on 18 June 1973 (Lemon and Burgess 1980). However, the El Reno storm had inbound velocities $>$100 m s^{-1} in its STD signature, which exceeds the 97 m s^{-1} observed in the Fort Cobb storm. The 150 m s^{-1} STD value is also more than double the median value of 72 m s^{-1} for STD observations from storms producing giant hail ($\geq$102 mm) in the study by Blair et al. (2011). Similarly for MRV, the maximum MRV of 42.5 m s^{-1} is nearly double the median value of 24 m s^{-1} for MRV observations from storms producing giant hail (Blair et al. 2011). And although the maximum value of MESH (121 mm) was lower than the observed size, such a high MESH should give adequate indication of the extreme nature of the threat.

In terms of the utility of the higher temporal resolution of the PAR vs the WSR-88D, this was most evident in the MESH and STD time series, with several instances of large increase or decrease in magnitude over short time intervals. Most notable is during the explosive growth phase and the transition into a classic supercell. In addition to providing earlier identification of significant changes in storm intensity, more frequent observation of important velocity signatures (such as STD and MRV) give end users greater confidence in the accuracy of their measured strength. This is particularly the case here, where the STD and MRV signatures had extremely high Doppler velocities involving extensive aliasing. When similar magnitude velocities are observed in STD or MRV signatures on consecutive volume scans over short time intervals (e.g., $<$1 min), the velocities are less likely to be spurious outliers. A recent experiment involving NWS forecasters confirmed that rapid-scan data improved their confidence in what they saw in the data (Heinselman et al. 2012).

Acknowledgments. The author thanks Rodger Brown for reviewing the paper.

References

Amburn, S. A., and P. L. Wolf, 1997: VIL density as a hail indicator. *Wea. Forecasting.*, **12**, 473–478, doi:10.1175/1520-0434(1997)012⟨0473:VDAAHI⟩2.0.CO;2.

Blair, S. F., D. R. Deroche, J. M. Boustead, J. W. Leighton, B. L. Barjenbruch, and W. P. Gargan, 2011: A radar-based assessment of the detectability of giant hail. *E-Journal of Severe Storms Meteorology*, **6 (7)**, 1–30, [Available online at http://www.ejssm.org/ojs/index.php/ejssm/article/view/87.].

Blair, S. F., and J. W. Leighton, 2012: Creating high-resolution hail datasets using social media and post-storm ground surveys. *Electronic J. Operational Meteor.*, **13**, 32–45.

Heinselman, P. L., D. S. LaDue, and H. Lazrus, 2012: Exploring impacts of rapid-scan radar data on NWS warning decisions. *Wea. Forecasting.*, **27**, 1031–1044, doi:10.1175/WAF-D-11-00145.1.

Hyvärinen, O., and E. Saltikoff, 2010: Social media as a source of meteorological observations. *Mon. Wea. Rev.*, **138**, 3175–3184, doi:10.1175/2010MWR3270.1.

Kumjian, M. R., and A. V. Ryzhkov, 2008: Polarimetric signatures in supercell thunderstorms. *J. Appl. Meteor. Climatol.*, **47**, 1940–1961, doi:10.1175/2007JAMC1874.1.

Lakshmanan, V., T. Smith, K. Hondl, G. J. Stumpf, and A. Witt, 2006: A real-time, three-dimensional, rapidly updating, heterogeneous radar merger technique for reflectivity, velocity, and derived products. *Wea. Forecasting.*, **21**, 802–823, doi:10.1175/WAF942.1.

Lakshmanan, V., T. Smith, G. Stumpf, and K. Hondl, 2007: The Warning Decision Support System – Integrated Information. *Wea. Forecasting.*, **22**, 596–612, doi:10.1175/WAF1009.1.

Lemon, L. R., and D. W. Burgess, 1980: Magnitude and implications of high speed outflow at severe storm summits. Preprints, *19th Conference on Radar Meteorology*, Miami Beach, FL, Amer. Meteor. Soc., 364–368.

Nelson, S. P., 1983: The influence of storm flow structure on hail growth. *J. Atmos. Sci.*, **40**, 1965–1983, doi:10.1175/1520-0469(1983)040%3C1965:TIOSFS%3E2.0.CO;2.

Rasmussen, E. N., and J. M. Straka, 1998: Variations in supercell morphology. Part I: Observations of the role of upper-level storm-relative flow. *Mon. Wea. Rev.*, **126**, 2406–2421, doi:10.1175/1520-0493(1998)126%3C2406:VISMPI%3E2.0.CO;2.

Witt, A., 1998: The relationship between WSR-88D measured midaltitude rotation and maximum hail size. Preprints, *19th Conference on Severe Local Storms*, Minneapolis, MN, Amer. Meteor. Soc., 740–743.

Witt, A., M. D. Eilts, G. J. Stumpf, J. T. Johnson, E. D. W. Mitchell, and K. W. Thomas, 1998: An enhanced hail detection algorithm for the WSR-88D. *Wea. Forecasting.*, **13**, 286–303, doi:10.1175/1520-0434(1998)013⟨0286:AEHDAF⟩2.0.CO;2.

Witt, A., and S. P. Nelson, 1991: The use of single-Doppler radar for estimating maximum hailstone size. *J. Appl. Meteor.*, **30**, 425–431, doi:10.1175/1520-0450(1991)030⟨0425:TUOSDR⟩2.0.CO;2.

Zrnic, D. S., and Coauthors, 2007: Agile-beam phased array radar for weather observations. *Bull. Amer. Meteor. Soc.*, **88**, 1753–1766, doi:10.1175/BAMS-88-11-1753.

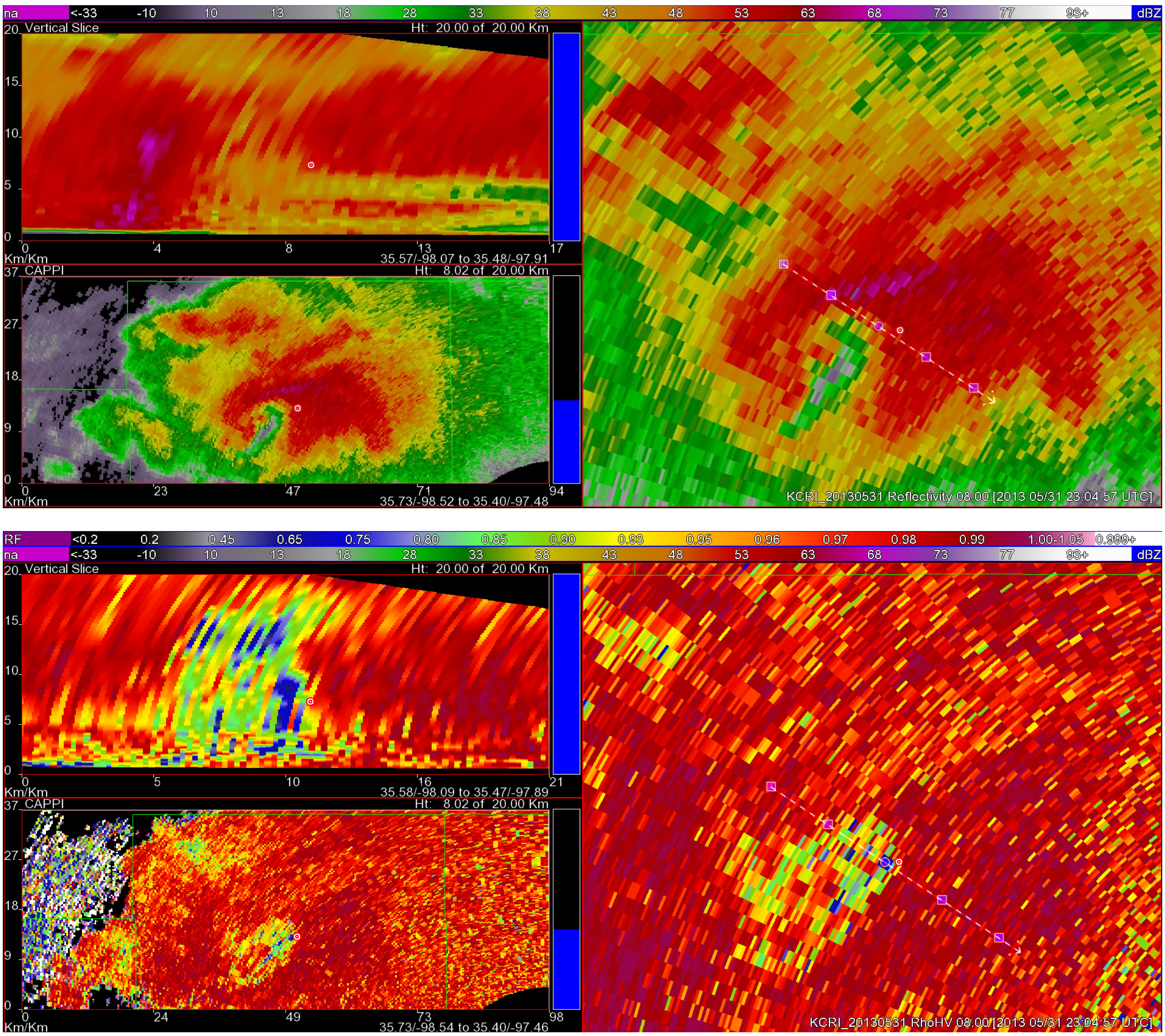

FIG. 2. Reflectivity (top 3 images) and cross-correlation coefficient (bottom 3 images) from the KCRI WSR-88D. Top color bar in the bottom figure shows cross-correlation coefficient values. For both the reflectivity and cross-correlation coefficient figures, the upper-left image is the vertical cross section along the dashed line shown on right-side image of the 8° elevation scan at 2305 UTC, and the lower-left image is the horizontal cross section at the 8 km AGL height. The red/white circle in the lower-left and right-side images is the location of the 160 mm hailstone.

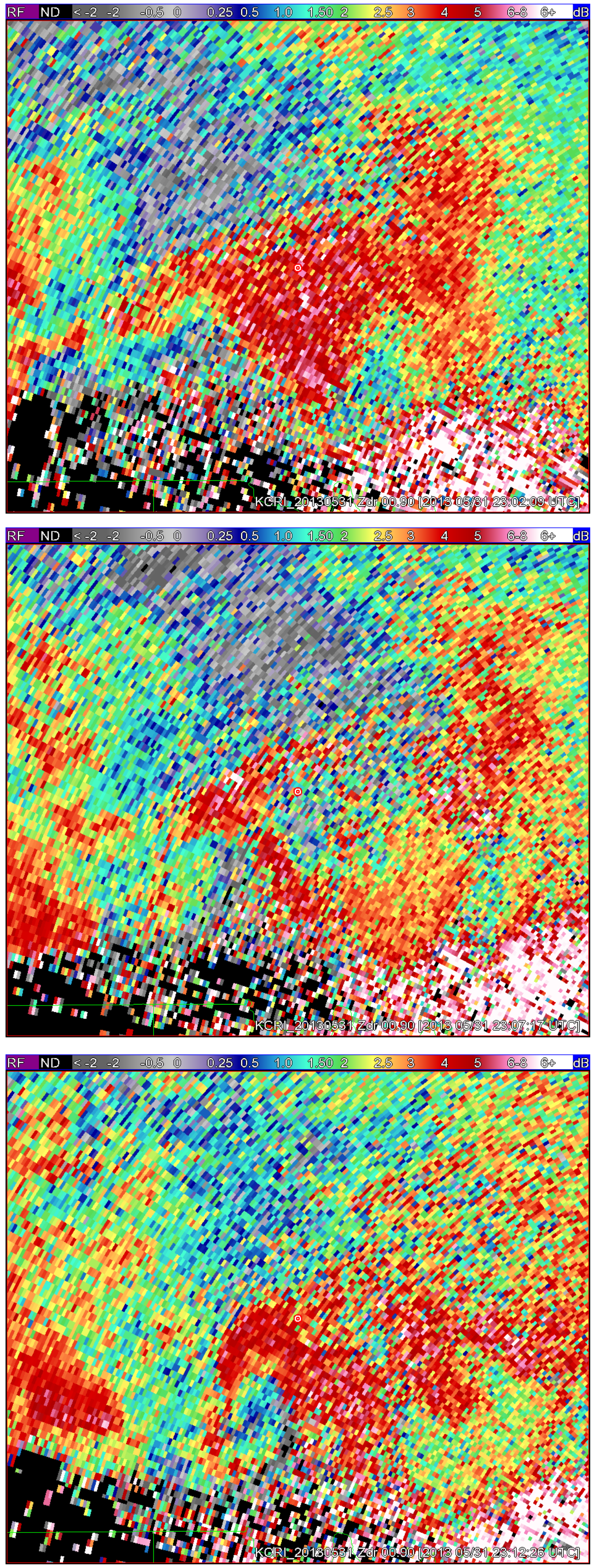

FIG. 3. Differential reflectivity from the KCRI WSR-88D for the 0.9° elevation scan at 2302 UTC (top), 2307 UTC (middle) and 2312 UTC (bottom). The red/white circle shows the location of the 160 mm hailstone.

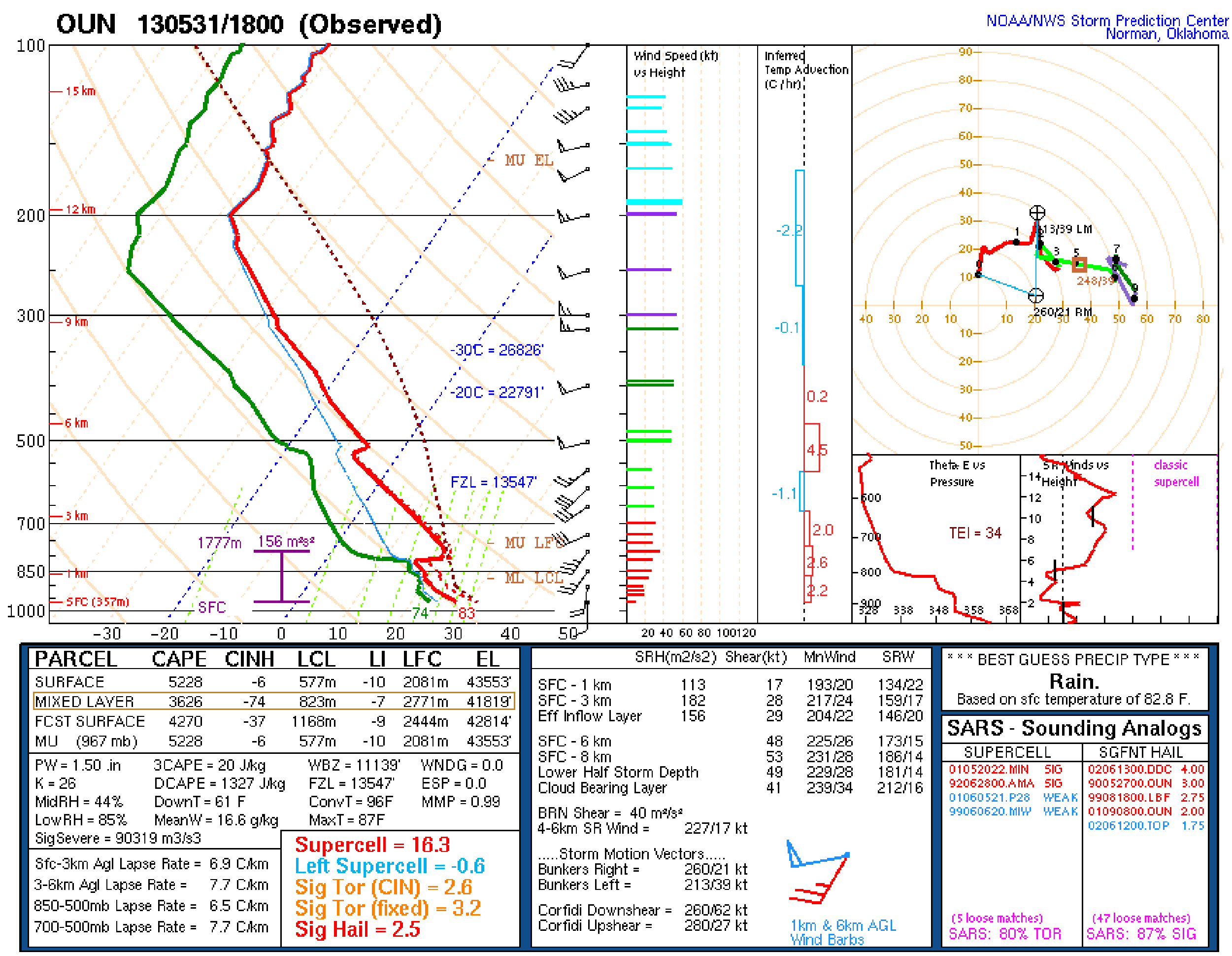

FIG. 4. OUN 1800 UTC rawinsonde.

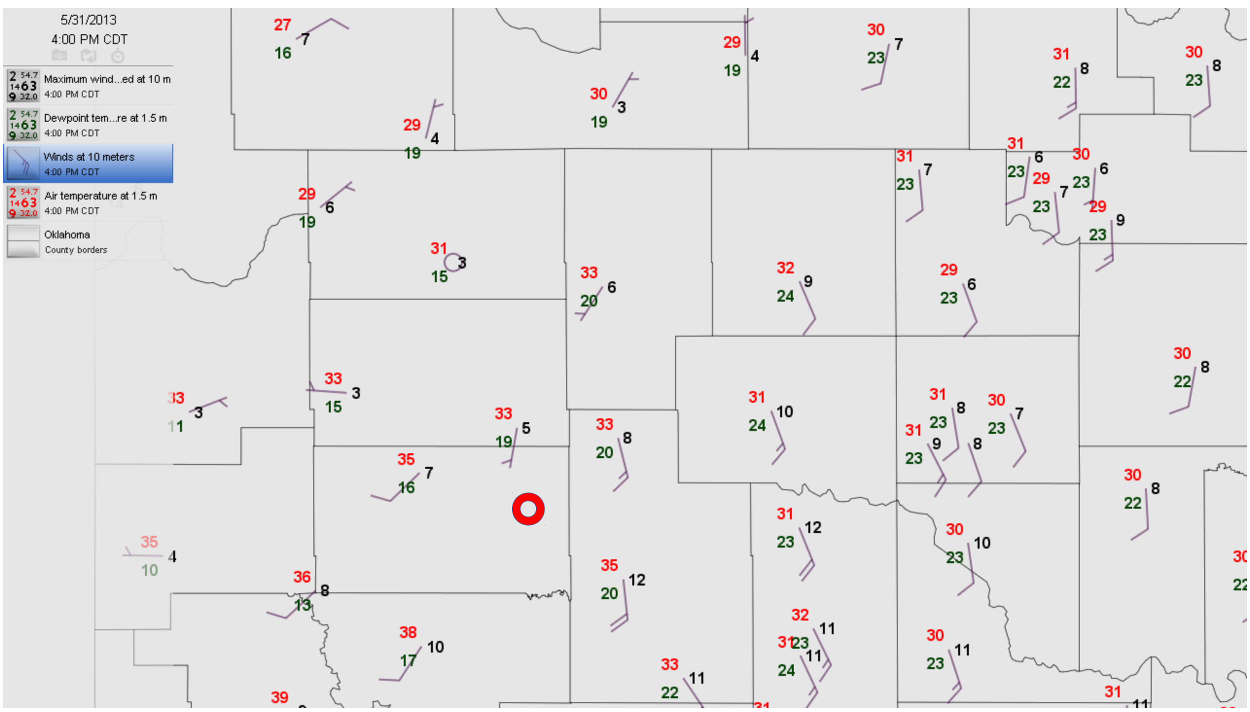

FIG. 5. Oklahoma Mesonet observations at 2100 UTC. Colored numerals show air temperature (°C): red, dewpoint temperature (°C): dark green, and maximum wind gust (highest 3-second wind speed, m s^{-1}): black. Wind barbs show 5-minute averaged wind; long barb: 5 m s^{-1}, short barb: 2.5 m s^{-1}. The red circle shows the first-echo location of the El Reno storm.

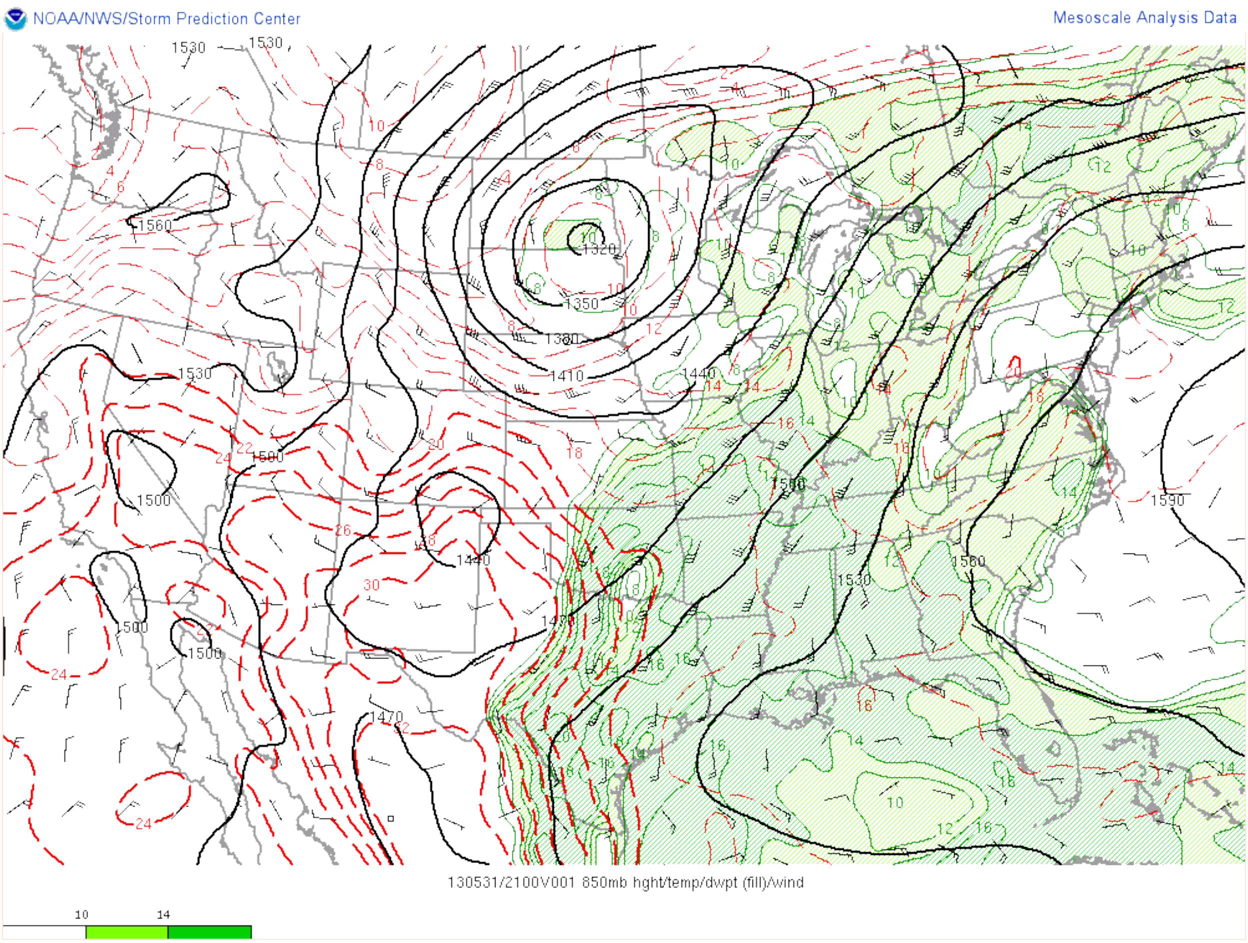

FIG. 6. SPC 850 mb analysis at 2100 UTC.

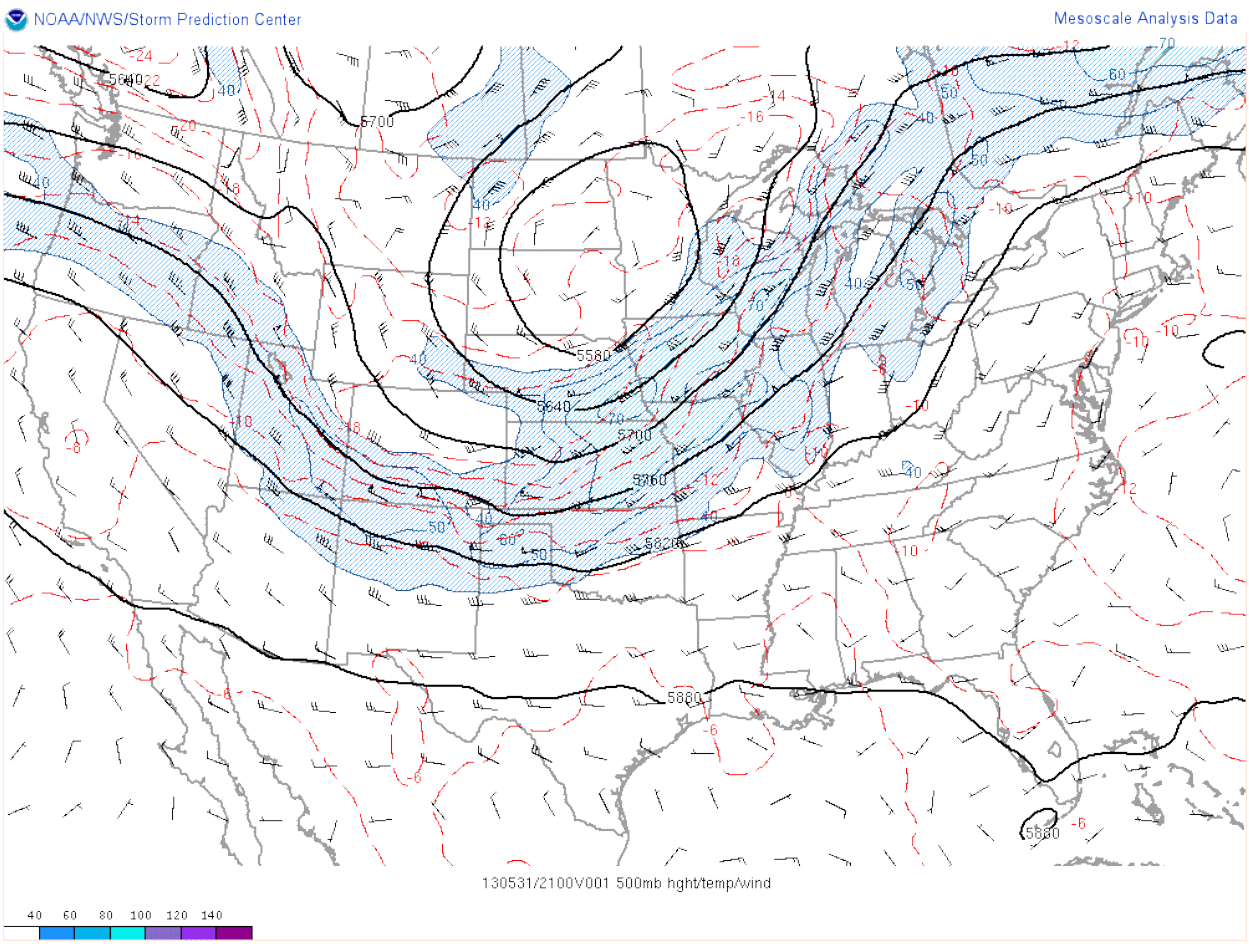

FIG. 7. SPC 500 mb analysis at 2100 UTC.

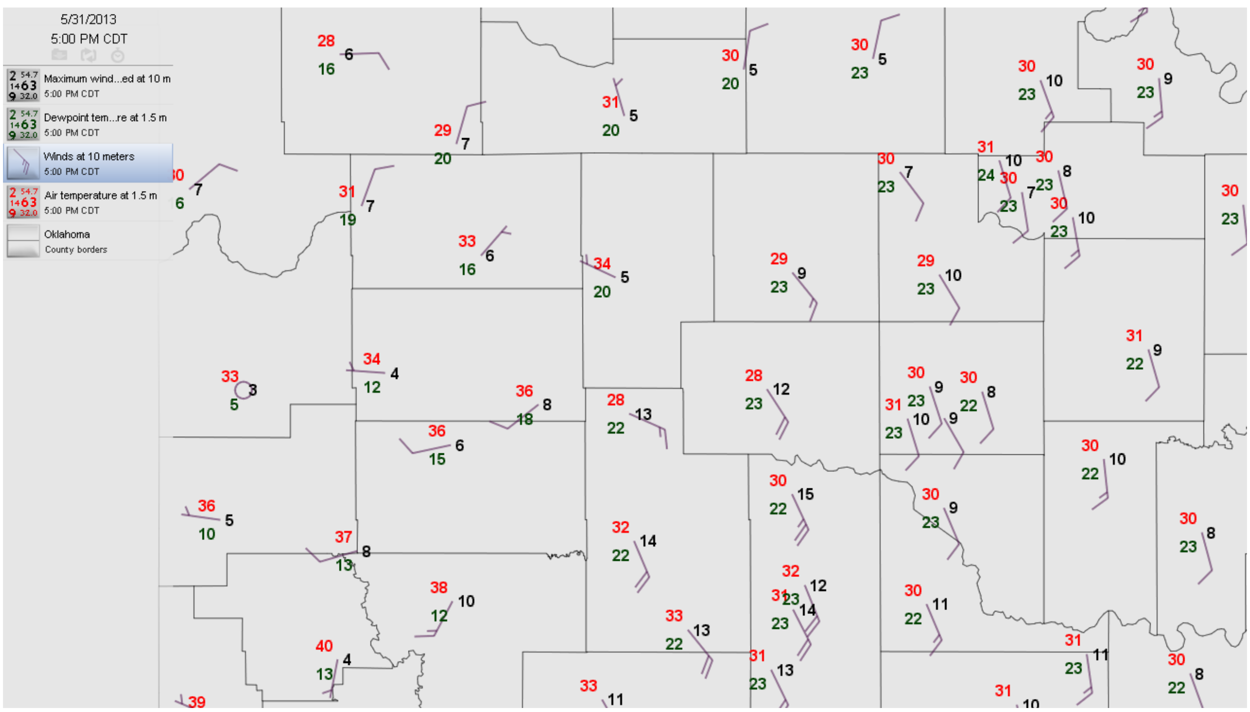

FIG. 8. Oklahoma Mesonet observations at 2200 UTC.

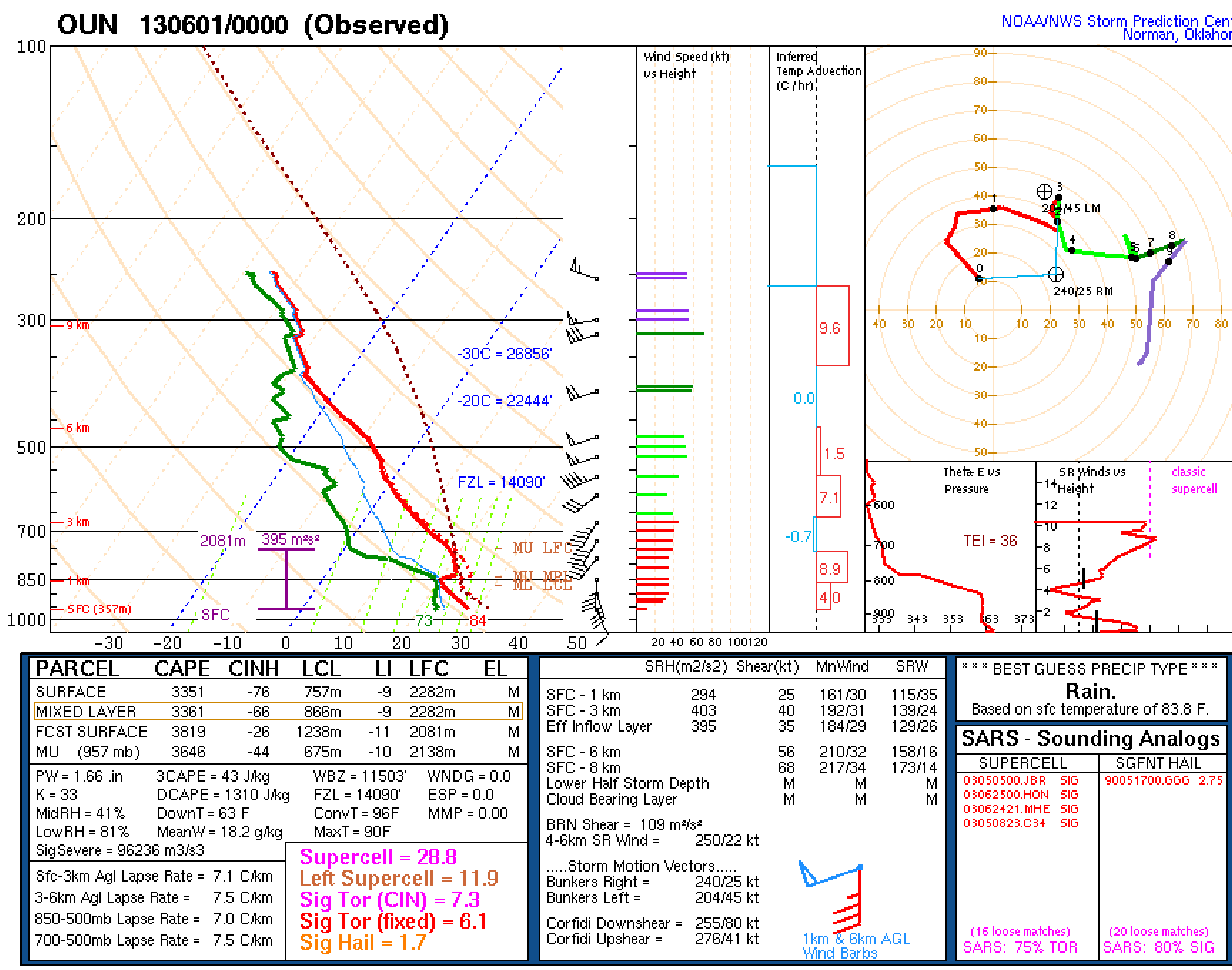

FIG. 9. OUN 0000 UTC rawinsonde.

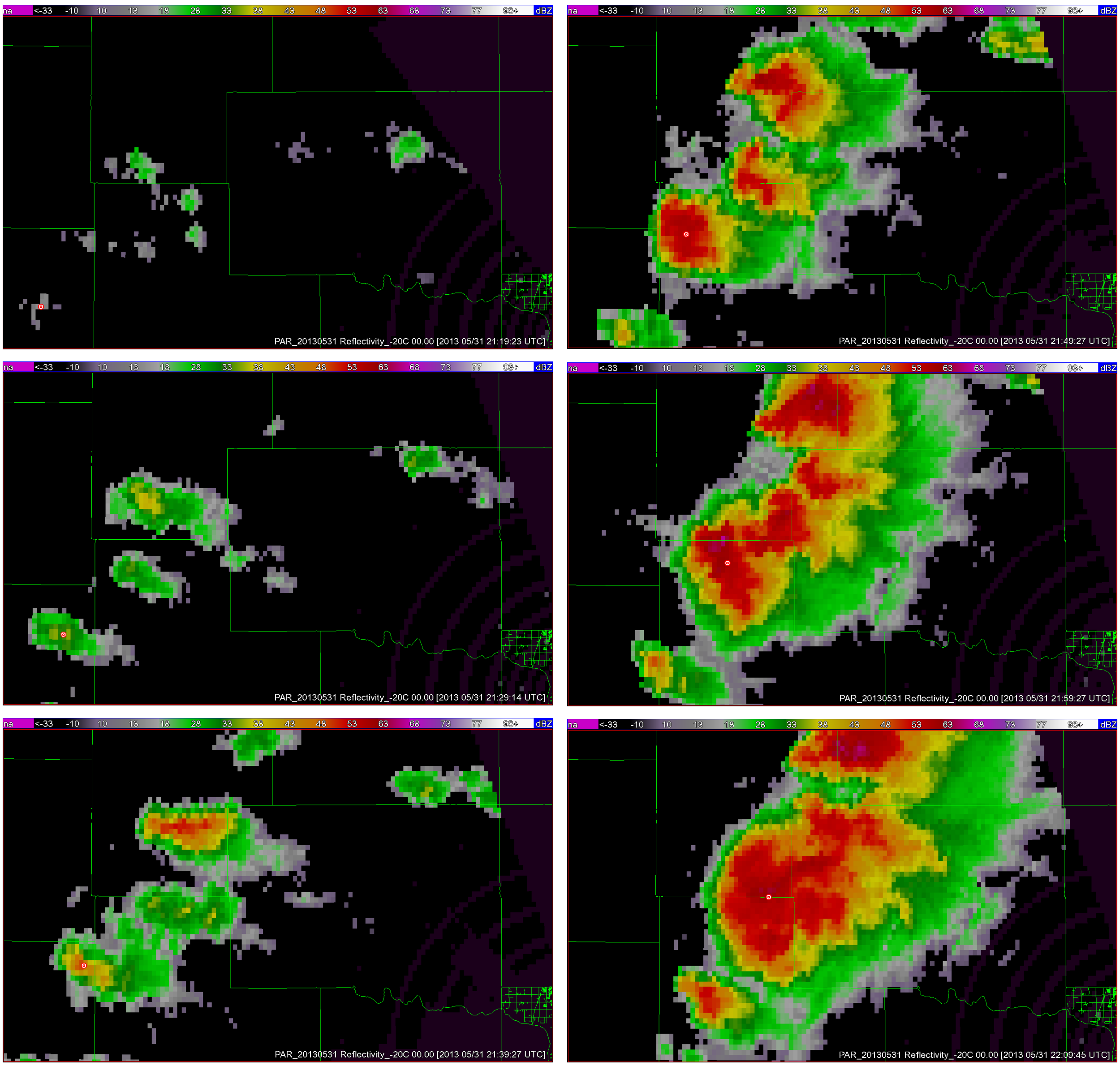

FIG. 10. PAR reflectivity at the -20°C height from first echo at 2119 UTC to 2210 UTC at $\sim$10 min intervals. Red/white circle shows location of the El Reno storm.

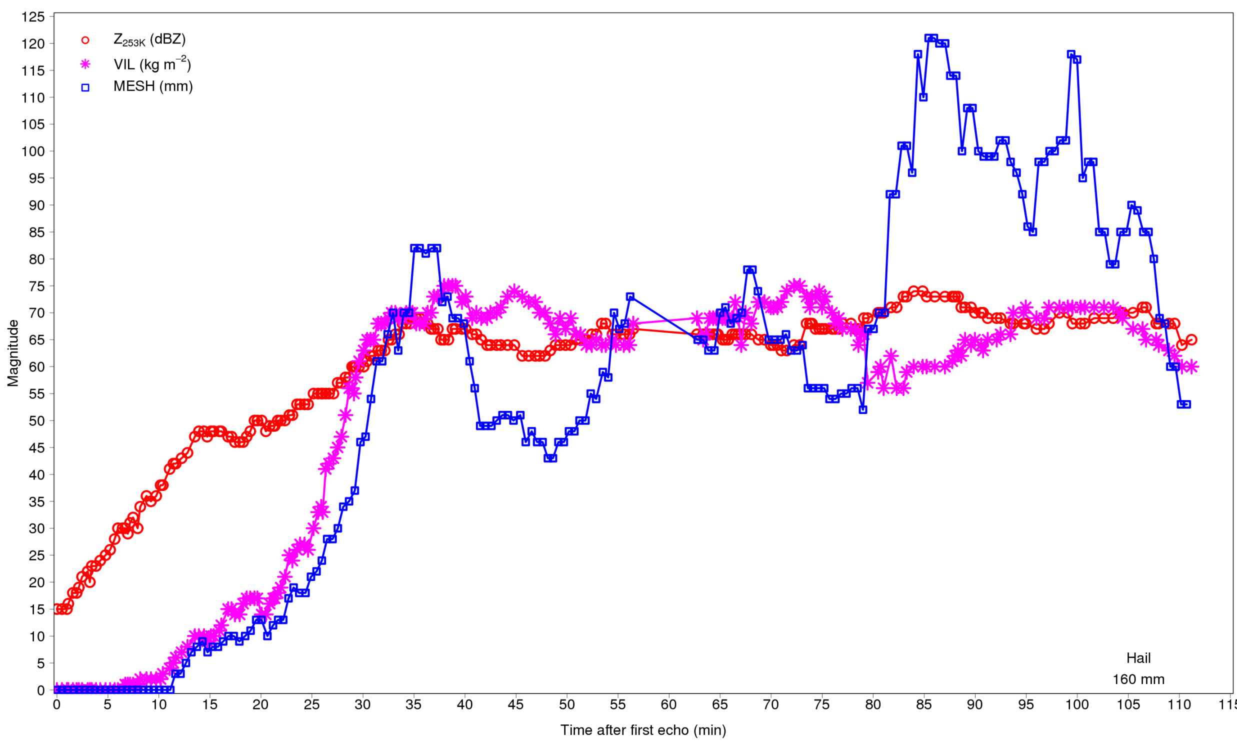

FIG. 11. Time series of Z_{253K}, VIL and MESH for the El Reno storm.

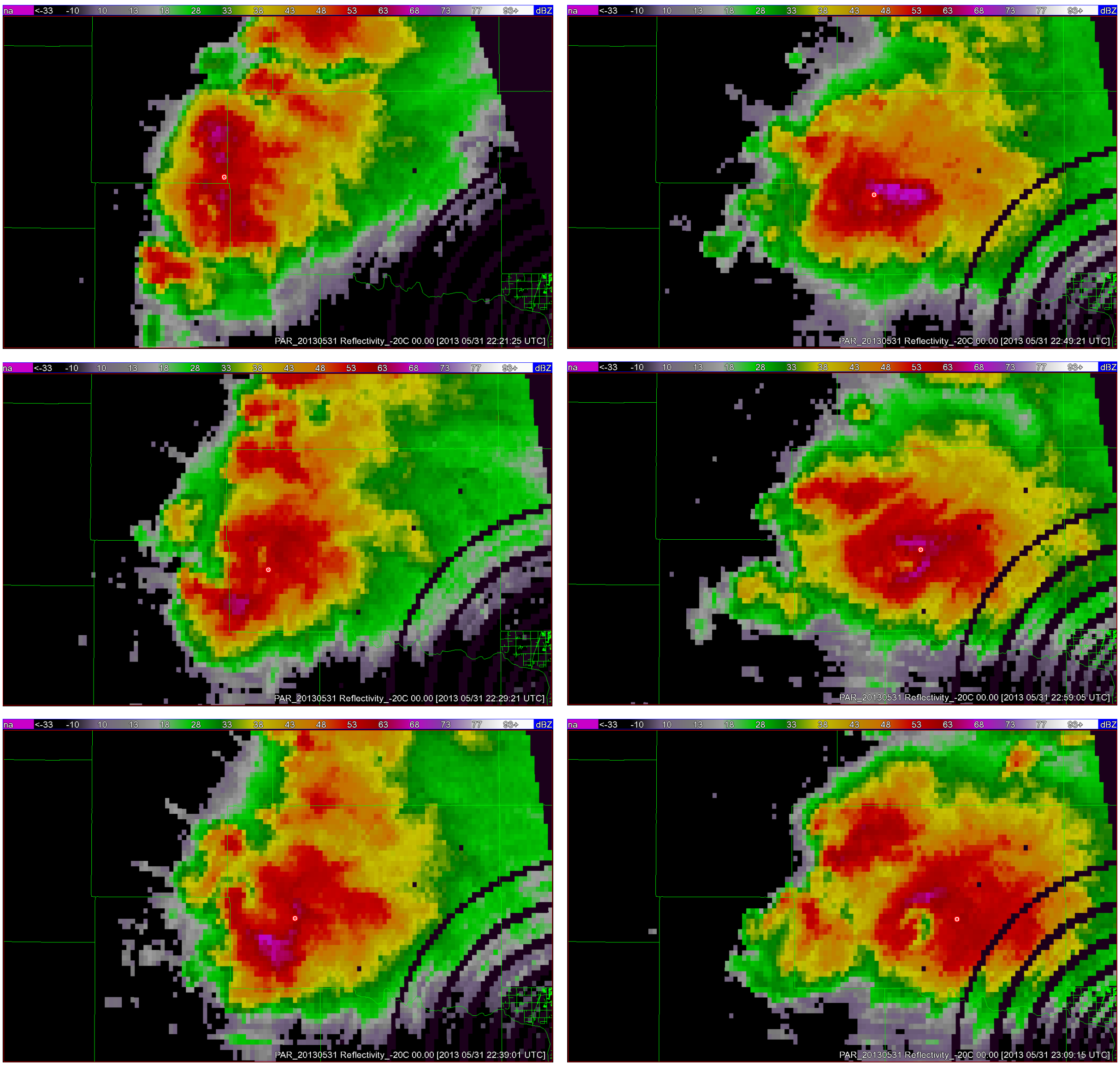

FIG. 12. PAR reflectivity at the -20°C height from 2221 UTC to 2309 UTC at $\sim$10 min intervals. Red/white circle shows location of the El Reno storm.

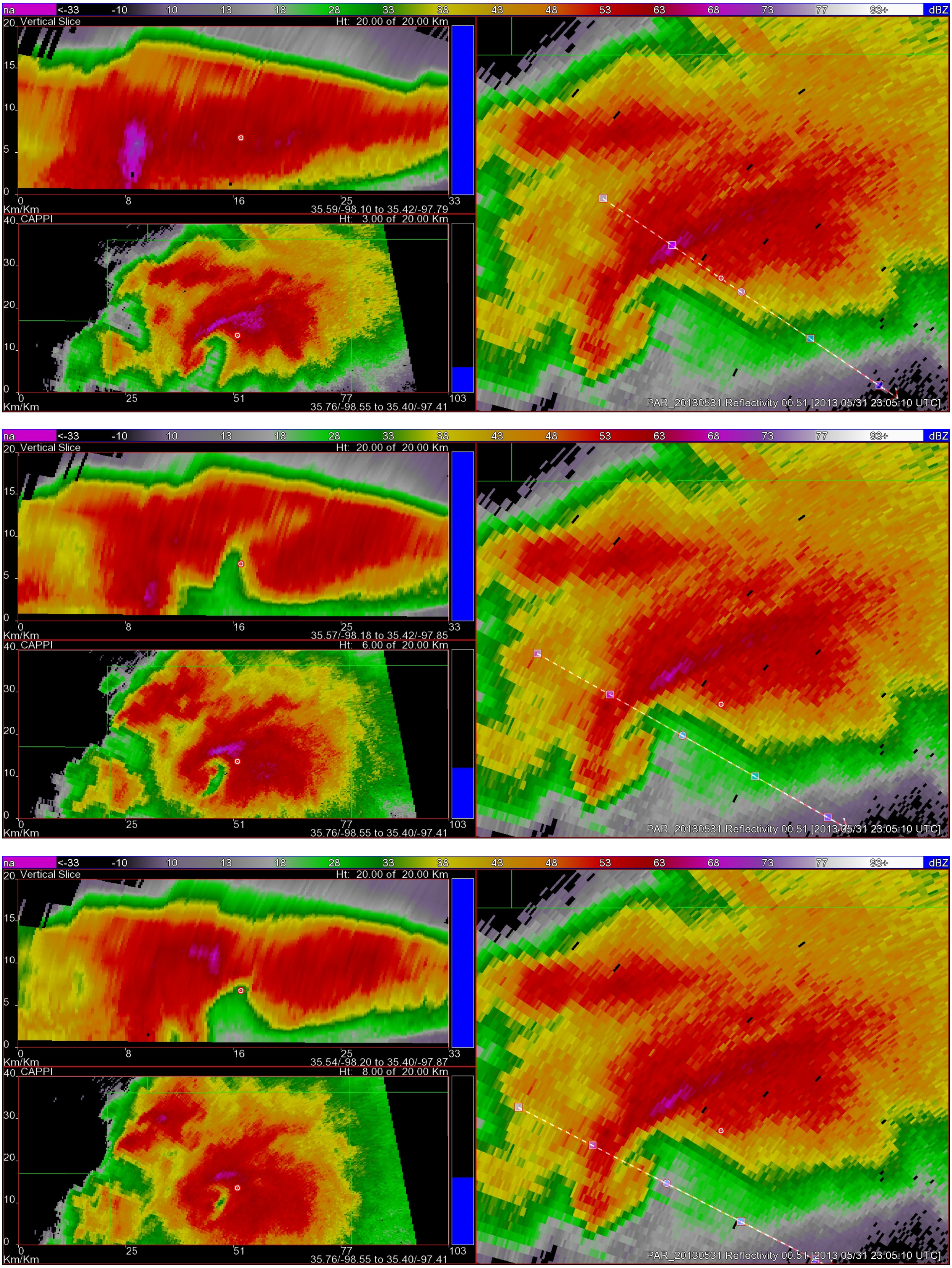

FIG. 13. PAR reflectivity structure of the El Reno storm at the time of the 160 mm hailstone. Dashed lines on right-side reflectivity images denote location of the vertical cross section shown in the corresponding upper-left images. Lower-left images are horizontal cross sections at heights of 3, 6 and 8 km AGL . The red/white circle in the lower-left and right-side images is the location of the 160 mm hailstone.

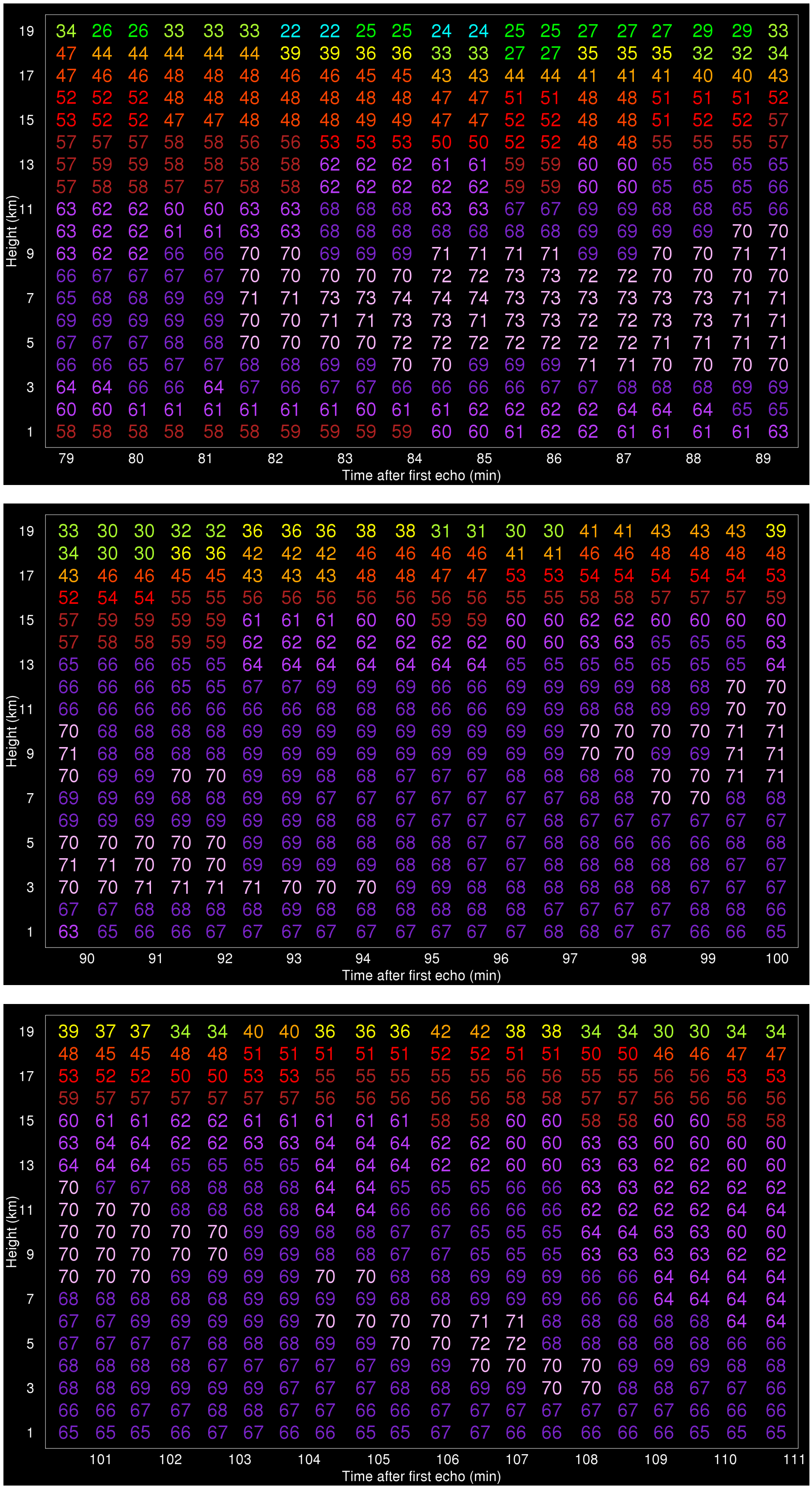

FIG. 14. Vertical reflectivity values (dBZ) used in the calculation of MESH around the time of the 160 mm hailstone (106 min AFE).

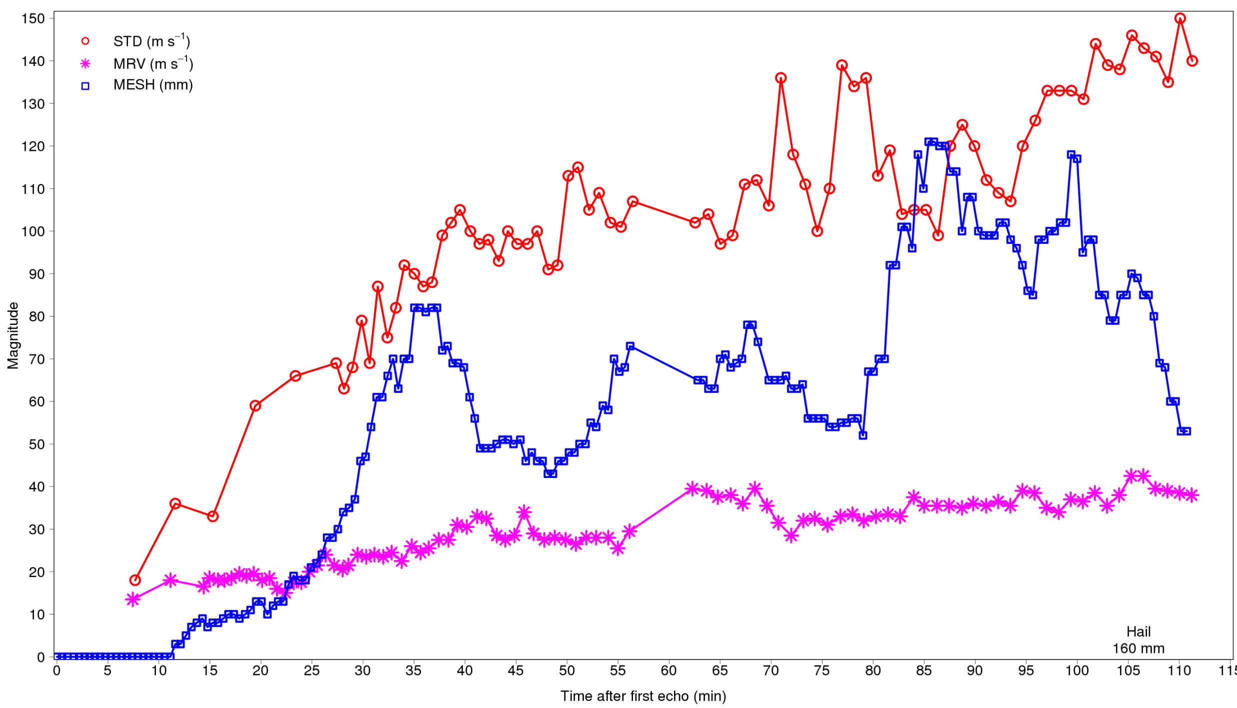

FIG. 15. Time series of STD, MRV and MESH for the El Reno storm. Due to range-folding of PAR velocity data, the first several STD and MRV measurements were obtained from the KTLX WSR-88D.